

Reference Signal Shaping for Closed-Loop Systems With Application to Seeking in Hard Disk Drives

Uwe Boettcher, *Student Member, IEEE*, Dirk Fetzer, *Student Member, IEEE*, Hui Li, Raymond A. de Callafon, and Frank E. Talke, *Fellow, IEEE*

Abstract—An input shaping algorithm based on convex optimization techniques is presented for the design of reference and feedforward signals in a closed-loop discrete-time linear time-invariant system. The proposed algorithm allows closed-loop signals to be subjected to linear constraints on amplitude and rate of change. As an illustrative example the seeking process in a hard disk drive is investigated. The closed-loop system response to both shaped and non-shaped inputs are compared. The computational scheme was experimentally tested on a modified hard disk drive.

Index Terms—Closed-loop systems, convex optimization, linear programming, matrix algebra, minimum-time control, multi-input/multi-output (MIMO) systems, quadratic programming, saturation control, set-point control, trajectory planning.

I. INTRODUCTION

FOR linear time-invariant (LTI) systems that are subject to a change from an initial state to a target state, input shaping is a powerful technique to reduce residual vibrations [1]. In this paper, we focus on reference signal input shaping for closed-loop systems with saturation constraints on the control output as indicated in Fig. 1. The targeting trajectory can be further optimized by minimizing targeting time, energy consumption or other system parameters, through convex optimization techniques. Those techniques have been widely applied to these problems since they guaranty convergence to a global optimum. In addition, recent increases in computational power in control systems justifies their increasing complexity. A broad overview of real-time or nearly real-time applications has been given in [2].

Input shaping is usually formulated as an open-loop problem where linear constraints on input and output signals are imposed to formulate a convex optimization problem to find optimal input profiles. In general, finite-impulse response (FIR) filters are used to pre-filter input signals such as shown for multiple-input multiple-output (MIMO) systems in continuous time in [3] and for discrete time systems in [4].

Manuscript received November 05, 2010; revised May 27, 2011; accepted October 25, 2011. Manuscript received in final form November 07, 2011. Date of publication December 13, 2011; date of current version February 01, 2012. Recommended by Associate Editor G. Cherubini.

U. Boettcher, D. Fetzer, R. A. de Callafon, and F. E. Talke are with the Department of Mechanical and Aerospace Engineering, Center for Magnetic Recording Research, University of California, San Diego, La Jolla, CA 92093-0401 USA (e-mail: uwe@ucsd.edu; dfetzer@ucsd.edu; callafon@ucsd.edu; ftalke@ucsd.edu).

H. Li is with the Storage Mechanics Laboratory, Hitachi Asia Ltd., 049318 Singapore (e-mail: hli@has.hitachi.com.sg).

Color versions of one or more of the figures in this paper are available online at <http://ieeexplore.ieee.org>.

Digital Object Identifier 10.1109/TCST.2011.2175733

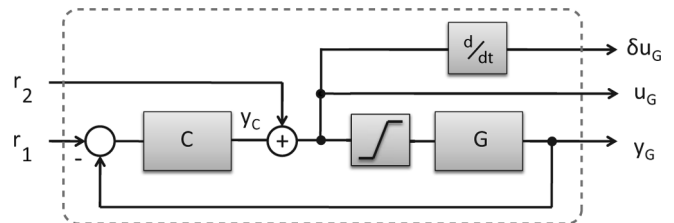


Fig. 1. Closed-loop LTI system with constraints on closed-loop signals.

Some closed-loop approaches are given in [5] where input shaping based on FIR filters is also applied to closed-loop systems. Another approach to closed-loop input shaping is the shaped time-optimal servo mechanism (STOS) approach that has been developed in [6] for continuous time systems. Here, mode switching control turns off the feedback during the targeting stage. In [7], the reference signal generation is shown for constrained closed-loop systems based on piecewise affine functions of state and reference. The conventionally shaped input signal tends to be longer than the non-shaped input signal as addressed in [8] where a solution to this problem is proposed. Another interesting approach to open-loop input shaping has been proposed in [9] where a graphical representation of the phase portrait is used to derive the input shaper. A low quantization level of the actuator signals (finite-state input) reduces the effectiveness of input shaping [10]. In [11]–[13], the reference signal generation is shown for a closed-loop system although time-minimal control is not addressed. It has been shown recently in [14] how an online optimization can yield improved performance compared to conventional input shapers.

Limited results are available on performing input shaping on closed-loop systems where reference and feedforward signals are computed in the presence of constraints on control and output signals. The computation of optimal reference profiles in closed-loop systems has direct application to high performance servo systems where short-time tracking of set-point values is required in the presence of saturation limits on control signals. A relevant application example is the servo mechanism in a hard disk drive (HDD). During the so-called track seeking process, the head is moved from one track to another. The hard disk drive servo mechanism faces several nonlinearities such as friction effects, or high frequency mechanical resonances [15]. However, the major nonlinearity that becomes apparent during the track-seeking mode is actuator saturation, i.e., the voice coil motor actuator has limits on its input and output. A number of different control schemes have been proposed to address this problem. One very popular technique is the so-called proximate time-optimal servo mechanism (PTOS) [16] that was modified from

conventional time-optimal control to apply a linear control law for small tracking errors. Another popular track-seeking control method is mode switching control with initial value compensation as proposed in the 1990s [17], [18]. Using this method, the transient behavior of the servo during the switching process between two controllers could be improved significantly. More recently, techniques such as composite nonlinear feedback (CNF) control [19] and the earlier mentioned STOS were proposed. A method addressing short distance seeks has been presented in [20] where step responses are shaped using initial value compensation of the feedback controller. Hence, no additional feed-forward control is needed and computational effort is therefore reduced. However, time-minimal control is not addressed in [20]. The computational framework presented here allows to compute reference signals for optimal seeking performance in hard drives. On the other hand, since the algorithm is applicable to a broad field of applications, we develop here a general input shaping technique for closed-loop MIMO linear time-invariant systems that use full degree-of-freedom control such as the one shown in Fig. 1. The algorithm computes the optimal reference signals r_1 and r_2 given linear constraints on the output signal y_G , the plant control signal u_G and the reference signals r_1 and r_2 . The simulated and experimentally verified results of the algorithm are applied in Section IV to the seeking process in a hard disk drive.

II. DEFINING THE SYSTEM

A. Specifications of Closed-Loop Signals

We consider a linear time-invariant model of the plant G in Fig. 1 with p inputs and m outputs of order n_G and an LTI model of the controller C with p outputs and m inputs of order n_C . The state space model of G is given by

$$\begin{aligned} x_G(k+1) &= A_G x_G(k) + B_G(r_2(k) + y_C(k)) \\ y_G(k) &= C_G x_G(k) + D_G(r_2(k) + y_C(k)) \end{aligned} \quad (1)$$

and the feedback connection is given by

$$\begin{aligned} x_C(k+1) &= A_C x_C(k) + B_C(r_1(k) - y_G(k)) \\ y_C(k) &= C_C x_C(k) + D_C(r_1(k) - y_G(k)). \end{aligned} \quad (2)$$

In order to specify constraints to the plant input, u_G and the rate of change δu_G must be available as outputs of the closed-loop state-space system as indicated in Fig. 1. Therefore, we add p states to the closed-loop model and define a measurement state vector x_M

$$x_M(k+1) = u_G(k) = y_C(k) + r_2(k) \quad (3)$$

and

$$u_G(k-1) = x_M(k). \quad (4)$$

We can now define the two additional outputs of our closed-loop system

$$\begin{aligned} u_G(k) &= y_C(k) + r_2(k) \\ \delta u_G(k) &= u_G(k) - u_G(k-1). \end{aligned} \quad (5)$$

Furthermore, we define the reference vector $r(k) \in \mathbb{R}^{(m+p) \times 1}$, the output vector $y(k) \in \mathbb{R}^{(m+2p) \times 1}$ and the state-space vector $x(k) \in \mathbb{R}^{(n_C+n_G+p) \times 1}$ as

$$r(k) = \begin{pmatrix} r_1 \\ r_2 \end{pmatrix} \quad y(k) = \begin{pmatrix} y_G \\ u_G \\ \delta u_G \end{pmatrix} \quad x(k) = \begin{pmatrix} x_C \\ x_G \\ x_M \end{pmatrix}. \quad (6)$$

Here, $r_1(k)$ and $r_2(k)$ are the computed reference signals.

Using (1)–(6) we can define the state space system of the closed-loop system as

$$\begin{aligned} x(k+1) &= Ax(k) + Br(k) \\ y(k) &= Cx(k) + Dr(k) \end{aligned} \quad (7)$$

where the state space matrices are calculated by

$$\begin{aligned} A &= \begin{bmatrix} A_C - B_C M D_G C_C & -B_C M C_G & 0 \\ B_G C_C - B_G D_C M D_G C_C & A_G - B_G D_C M C_G & 0 \\ C_C - D_C M D_G C_C & -D_C M C_G & 0 \end{bmatrix} \\ B &= \begin{bmatrix} B_C - B_C M D_G D_C & -B_C M D_G \\ B_G D_C - B_G D_C M D_G D_C & B_G - B_G D_C M D_G \\ D_C - D_C M D_G D_C & -D_C M D_G + I \end{bmatrix} \\ C &= \begin{bmatrix} M D_G C_C & M C_G & 0 \\ C_C - D_C M D_G C_C & -D_C M C_G & 0 \\ C_C - D_C M D_G C_C & -D_C M C_G & -I \end{bmatrix} \\ D &= \begin{bmatrix} M D_G D_C & M D_G \\ D_C - D_C M D_G D_C & I - D_C M D_G \\ D_C - D_C M D_G D_C & I - D_C M D_G \end{bmatrix}. \end{aligned} \quad (8)$$

In (8), M is defined as

$$M = (I + D_G D_C)^{-1}. \quad (9)$$

The inverse in (9) can be calculated for a well-defined closed-loop system with $D_G D_C \neq -I$. In practical applications most plants will have at least one sample time delay with $D_G = 0$ making $M = I$.

B. Explicit Solution of the Closed-Loop System

The output y combines the plant output y_G , the plant input u_G and its rate of change δu_G on which constraints will be imposed. For the formulation of the linear constraints we use (7) and follow [21] (but including the feed-through term D) to write the output equations recursively as

$$\begin{aligned} y(0) &= Cx(0) + Dr(0) \\ y(1) &= CAx(0) + CBr(0) + Dr(1) \\ y(2) &= CA^2x(0) + CABr(0) + CBr(1) + Dr(2) \\ &\vdots \\ y(M) &= CA^M x(0) + \sum_{i=1}^M CA^{M-i} Br(i-1) + Dr_s \\ y(M+1) &= CA^{M+1} x(0) \\ &\quad + \sum_{i=1}^M CA^{M+1-i} Br(i-1) + Dr_s + CBr_s \end{aligned}$$

$$\begin{aligned}
& \vdots \\
y(N-1) &= CA^{N-1}x(0) + \sum_{i=1}^M CA^{N-i-1}Br(i-1) + \\
& \quad + Dr_s + \sum_{i=1}^{N-M-1} CA^{i-1}Br_s
\end{aligned} \quad (10)$$

where M is the control horizon and N is the optimization horizon. Here, r_s defines the residual reference signal after the control horizon which in our work is set to a constant desired value. An obvious choice is $r_1 = y_t$ and $r_2 = 0$ for $k \geq M$ where y_t represents the target value of the output.

We can now rewrite (10) conveniently in matrix notation by defining Ψ as

$$\Psi = \begin{bmatrix} D & 0 & 0 & \dots & 0 \\ CB & D & 0 & \dots & 0 \\ CAB & CB & D & \dots & 0 \\ \vdots & \vdots & \vdots & \ddots & \vdots \\ CA^{M-2}B & CA^{M-3}B & \dots & \dots & D \\ CA^{M-1}B & CA^{M-2}B & \dots & \dots & CB \\ CA^M B & CA^{M-1}B & \dots & \dots & CAB \\ \vdots & \vdots & \ddots & \vdots & \vdots \\ CA^{N-2}B & CA^{N-3}B & \dots & CA^{N-M-1}B & \end{bmatrix}. \quad (11)$$

Furthermore, we define Ω , \mathbf{y} and Δ as

$$\Omega = \begin{bmatrix} C \\ CA \\ CA^2 \\ \vdots \\ CA^{N-1} \end{bmatrix}, \mathbf{y} = \begin{bmatrix} y(0) \\ y(1) \\ y(2) \\ \vdots \\ y(N-1) \end{bmatrix}$$

$$\Delta = \begin{bmatrix} 0 \\ \vdots \\ 0 \\ Dr_s \\ Dr_s + CB r_s \\ \vdots \\ Dr_s + \sum_{i=1}^{N-M-1} CA^{i-1}Br_s \end{bmatrix}. \quad (12)$$

With this definition we can rewrite (10) as

$$\mathbf{y} = \Psi \mathbf{r} + \underbrace{\Omega x(0) + \Delta}_{\mathbf{q}} \quad (13)$$

where the vector \mathbf{r} contains the reference signals

$$\mathbf{r} = [r(0), \dots, r(M-1)]^T \quad (14)$$

and the vector \mathbf{y} contains the output signals

$$\mathbf{y} = [y(0), \dots, y(N-1)]^T \quad (15)$$

for each time step k . In (13), we also introduce \mathbf{q} that captures the residual and initial condition. Each element in (14) is a

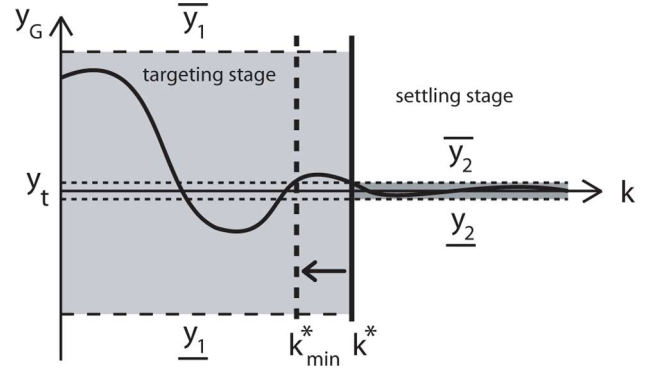


Fig. 2. Definition of the output constraints.

vector of size $(m+p) \times 1$, and, each element in (15) is a vector of size $(m+2p) \times 1$. In (13), the explicit input-output relation is linear in \mathbf{r} . We shall now proceed to specify the constraints and the optimization routine for reference signal shaping.

III. CONVEX OPTIMIZATION

For a comprehensive overview of convex optimization techniques the reader is referred to [22]. In this paper a specific solution to the closed-loop problem will be given for designing the reference signal \mathbf{r} subjected to constraints on the closed-loop signals and the reference signals (6).

A. Constraints on the Closed-Loop Signals

As indicated in Fig. 1, the output y captures all of the relevant closed-loop signals. It contains not only the output of the plant y_G but also the plant input u_G and its rate of change δu_G . In defining constraints on closed-loop signals we refer to the constraints on the output $y = (y_G, u_G, \delta u_G)^T$ in which we distinguish between different signals. The plant output y_G is subject to two different amplitude constraints as indicated in Fig. 2. One constraint is a large amplitude constraint during the targeting stage. We define the maximum and minimum constraints by $\overline{y_1}$ and $\underline{y_1}$, respectively. Once the target is reached, a tolerance ϵ of the output from the desired target is specified by

$$\underline{y_2} = y_t - \epsilon \leq y_G \leq \overline{y_2} = y_t + \epsilon \quad (16)$$

creating a tight amplitude constraint during the settling stage. In Fig. 2, k^* denotes the number of samples to reach the target. For all sample numbers $k < k^*$ the targeting output constraints apply, while for all sample numbers $k \geq k^*$ the settling stage (and finally steady state) output constraints apply. Choosing a minimal value for k^* would amount to finding a minimal time solution. We will later use a line search over k^* to find the minimal time solution. For now, k^* is assumed to be given.

Furthermore, we specify constraints on the plant input u_G . We consider amplitude constraints on the input. In addition, the maximum rate of change of the input signal is limited which is commonly introduced through rate limitations in digital-to-analog conversion. We define amplitude and rate constraints as

$$u_G \leq \overline{u_G} \quad \delta u_G \leq \overline{\delta u_G} \quad (17)$$

and similarly

$$\begin{aligned} u_G \geq \underline{u}_G &\Leftrightarrow -u_G \leq -\underline{u}_G \\ \delta u_G \geq \underline{\delta u}_G &\Leftrightarrow -\delta u_G \leq -\underline{\delta u}_G. \end{aligned} \quad (18)$$

In matrix notation the output constraints can be written as

$$\Psi \mathbf{r} + \mathbf{q} \leq \bar{\mathbf{y}}(k^*) \quad (19)$$

and

$$\Psi \mathbf{r} + \mathbf{q} \geq \underline{\mathbf{y}}(k^*) \quad (20)$$

where \mathbf{q} is given in (13) and $\bar{\mathbf{y}}$ and $\underline{\mathbf{y}}$ are defined by

$$\bar{\mathbf{y}}(k^*) = \begin{bmatrix} \bar{y}_1 \\ \underline{u}_G \\ \delta u_G \\ \vdots \\ \bar{y}_2 \\ \underline{u}_G \\ \delta u_G \end{bmatrix}, \underline{\mathbf{y}}(k^*) = \begin{bmatrix} \underline{y}_1 \\ \underline{u}_G \\ \underline{\delta u}_G \\ \vdots \\ \underline{y}_2 \\ \underline{u}_G \\ \underline{\delta u}_G \end{bmatrix}. \quad (21)$$

B. Constraints on Reference Signals

The reference signals r_1 and r_2 in Fig. 1 are captured in the signal r in (7) and (14). By imposing constraints on \mathbf{r} we are now referring to the constraints on the reference inputs r_1 and r_2 . The reference signals are limited by an amplitude constraint

$$\underline{\mathbf{r}} \leq \mathbf{r} \leq \bar{\mathbf{r}} \quad (22)$$

whereas a rate of change constraint

$$\underline{\delta \mathbf{r}} \leq \delta \mathbf{r} \leq \bar{\delta \mathbf{r}} \quad (23)$$

with

$$\bar{\mathbf{r}} = [\bar{r}, \dots, \bar{r}]^T \quad (24)$$

$$\bar{\delta \mathbf{r}} = [\bar{\delta r}, \dots, \bar{\delta r}]^T \quad (25)$$

can also be included in our approach. We note that $\underline{\mathbf{r}}$ and $\underline{\delta \mathbf{r}}$ are defined similarly.

A reference change is defined by

$$\delta r(k) = r(k) - r(k-1) \quad (26)$$

for each $k \in [0, \dots, M-1]$. In matrix notation we calculate $\delta \mathbf{r}$ by

$$\delta \mathbf{r} = \mathbf{E} \mathbf{r} \quad (27)$$

where \mathbf{E} is given by

$$\mathbf{E} = \begin{bmatrix} I_{m+p} & 0 & \dots & 0 \\ -I_{m+p} & I_{m+p} & \dots & 0 \\ & \ddots & \ddots & \\ 0 & \dots & -I_{m+p} & I_{m+p} \end{bmatrix} \quad (28)$$

and I_{m+p} represents a $(m+p) \times (m+p)$ identity matrix.

TABLE I
BISECTION ALGORITHM

```

 $k_{\text{upper}}^* = M$ 
 $k_{\text{lower}}^* = 1$ 
while ( $k_{\text{upper}}^* - k_{\text{lower}}^* > 1$ )
     $k^* = \frac{k_{\text{upper}}^* + k_{\text{lower}}^*}{2}$ 
    solve LP in (31) with  $k^*$ 
    if LP feasible
         $k_{\text{upper}}^* = k^*$ 
    else
         $k_{\text{lower}}^* = k^*$ 
    end if
end
 $k_{\text{min}}^* = k_{\text{upper}}^*$ 

```

C. Combined Constraint in Linear Form

All the constraints in (19), (20), (22), (23) and (27) can be combined in one single linear matrix inequality (LMI):

$$\begin{bmatrix} \mathbf{I} \\ -\mathbf{I} \\ \mathbf{E} \\ -\mathbf{E} \\ \Psi \\ -\Psi \end{bmatrix} \begin{bmatrix} r(0) \\ \vdots \\ r(M-1) \end{bmatrix} \leq \begin{bmatrix} \bar{\mathbf{r}} \\ -\underline{\mathbf{r}} \\ \delta \mathbf{r} \\ -\delta \mathbf{r} \\ \bar{\mathbf{y}}(k^*) \\ -\underline{\mathbf{y}}(k^*) \end{bmatrix} - \begin{bmatrix} 0 \\ 0 \\ 0 \\ 0 \\ \mathbf{q} \\ -\mathbf{q} \end{bmatrix} \quad (29)$$

or short

$$\mathbf{L} \mathbf{r} \leq \mathbf{W}(k^*) - \mathbf{Q}. \quad (30)$$

In (29), \mathbf{I} is an $(m+p)M \times (m+p)M$ identity matrix, and Ψ is given in (11). In (29) and (30), the term \mathbf{Q} with $\mathbf{q} = \Omega x(0) + \Delta$ represents the effect of initial and residual conditions. It should be noted that \mathbf{W} depends on the choice of k^* in Fig. 2. The additional freedom in k^* will be used to check for a feasible solution of the input shaping problem and to formulate a minimal time solution for settling.

D. Feasibility Check for Time-Optimal Solution

We can check whether or not the constraints are feasible for a given k^* by solving a relatively simple linear program (LP) [23], [24]

$$\begin{aligned} \min_{\mathbf{r}, \mathbf{z}} \quad & \mathbf{1}^T \mathbf{z} \\ \text{subject to} \quad & \mathbf{L} \mathbf{r} - \mathbf{z} \leq \mathbf{W}(k^*) - \mathbf{Q} \\ & \mathbf{z} \geq 0. \end{aligned} \quad (31)$$

If $\mathbf{z} = 0$ is the optimal solution then the inequality (30) is feasible, otherwise infeasible. In (31), $\mathbf{1} = [1, \dots, 1]^T$ is a column vector of ones.

In order to obtain the time-optimal solution we solve the LP in (31) several times for different values of k^* . We use a bisection method [22] that results in quadratic convergence to find the minimum sample number k_{min}^* (where $1 \leq k_{\text{min}}^* \leq M$) for a feasible set of constraints. The pseudo code of the bisection algorithm is listed in Table I.

The bisection algorithm to find k_{min}^* leads also to a computed reference signal \mathbf{r} that satisfies all imposed constraints. The LP program in (31) is used only to check the feasibility of the pro-

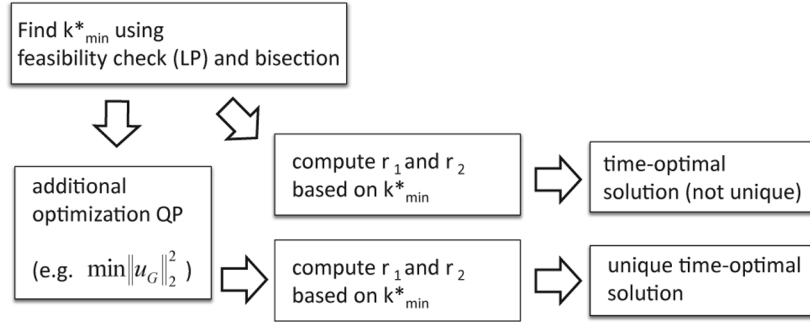


Fig. 3. Optimization algorithm.

posed reference signal shaping under the given constraints. The additional bisection in Table I will also allow us to find the minimal time solution that is still feasible.

It should be noted that the solution for \mathbf{r} found by (31) is not unique and most likely will not be a desired reference signal. Moreover, in many applications a minimum time solution might not be required. Given the feasibility check from the LP problem we now design a unique reference signal by posing a quadratic programming (QP) problem as indicated in Fig. 3 that aims at minimizing the (weighted) energy level of the signals, leading to a unique solution of the reference signal \mathbf{r} .

E. Quadratic Programming (QP)

To further improve the energy properties of the signals in the input shaping problem one can pose a quadratic criterion involving both \mathbf{y} and \mathbf{r} given the constraints in (29) and (30). A particular value for k^* can give a feasible solution from the LP problem in (31) and a further refinement of this solution can be found by solving the QP problem

$$\begin{aligned} \min_{\mathbf{r}, \mathbf{y}'} \quad & \mathbf{y}'^T \mathbf{P}_1 \mathbf{y}' + \mathbf{r}^T \mathbf{P}_2 \mathbf{r} \\ \text{subject to} \quad & \mathbf{Lr} \leq \mathbf{W}(k^*) \mathbf{Q} \\ & \mathbf{y}' = \mathbf{\Psi} \mathbf{r} + \mathbf{q} - \mathbf{y}_t^* \end{aligned} \quad (32)$$

where \mathbf{y}_t^* is defined by

$$\mathbf{y}_t^* = [y_t \ 0 \ 0 \ \cdots \ y_t \ 0 \ 0]^T. \quad (33)$$

In (32), \mathbf{P}_1 and \mathbf{P}_2 are semi-positive definite matrices with dimensions of \mathbf{y}' and \mathbf{r} , respectively. With $\mathbf{P}_1 \geq 0$ and $\mathbf{P}_2 \geq 0$, the QP problem is convex. The QP in (32) consists of a quadratic cost function, an inequality constraint linear in \mathbf{r} and an equality constraint linear in \mathbf{r} and \mathbf{y}' .

The introduction of the additional variable \mathbf{y}' and the equality constraint is necessary in order to perform optimization on y_G , u_G and δu_G .

The QP in (32) represents only one possible optimization objective but there are many other possible objectives. The weighting matrices \mathbf{P}_1 and \mathbf{P}_2 allow an accurate tuning according to the desired closed-loop response also depending on k . If only some of the constraints in (29) are in use, the problem size should be reduced in favor of shorter computational time.

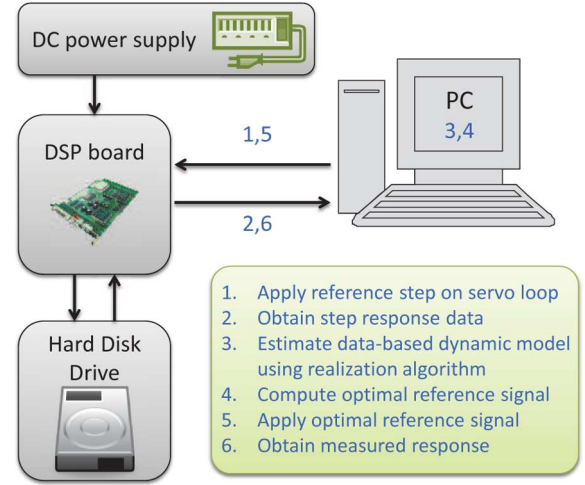


Fig. 4. Computational steps and scheme of the experimental setup.

F. Semidefinite Programming (SDP)

The quadratic programming problem in (32) can be reformulated as a SDP problem that can be considered as an extension of linear programming [25]. First, the equality constraint is incorporated in the cost function J which yields the QP

$$\begin{aligned} \min_{\mathbf{r}} \quad & J \\ \text{subject to} \quad & \mathbf{Lr} \leq \mathbf{W}(k^*) - \mathbf{Q} \end{aligned} \quad (34)$$

where J is defined by

$$\begin{aligned} J = & \mathbf{r}^T \underbrace{\left(\mathbf{\Psi}^T \mathbf{P}_1 \mathbf{\Psi} + \mathbf{P}_2 \right)}_{\Theta_1} \mathbf{r} + \underbrace{\left(\mathbf{q}^T - \mathbf{y}_t^{*T} \right)}_{\Theta_3} \mathbf{P}_1 \mathbf{\Psi} \mathbf{r} \\ & + \mathbf{r}^T \underbrace{\mathbf{\Psi}^T \mathbf{P}_1}_{\Theta_3^T} \left(\mathbf{q} - \mathbf{y}_t^* \right) \\ & + \underbrace{\left(\mathbf{q}^T - \mathbf{y}_t^{*T} \right)}_{\Theta_2} \mathbf{P}_1 \left(\mathbf{q} - \mathbf{y}_t^* \right). \end{aligned} \quad (35)$$

Suppose γ is the upper bound on J we can rewrite (34) as

$$\begin{aligned} \min_{\mathbf{r}, \gamma} \quad & \gamma \\ \text{subject to} \quad & \gamma - J \geq 0 \\ & \mathbf{Lr} \leq \mathbf{W}(k^*) - \mathbf{Q}. \end{aligned} \quad (36)$$

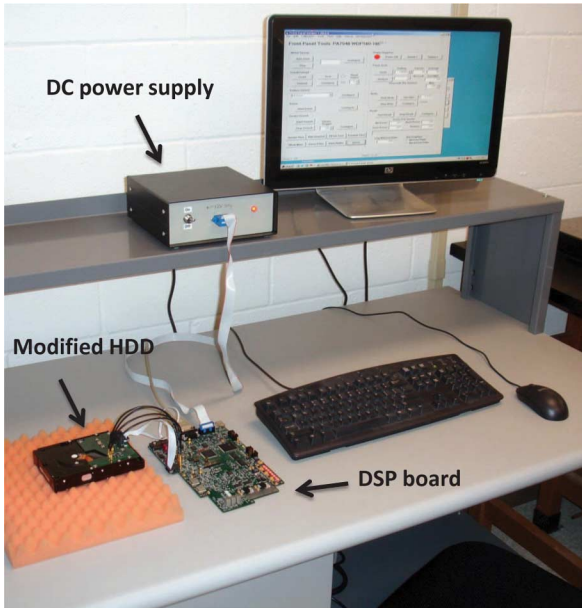


Fig. 5. Experimental setup: Modified HDD, DSP board, DC power supply, and computer.

If $P_1 \succ 0$ and/or $P_2 \succ 0$ holds, the inverse of Θ_1 in (35) is defined and we can apply the Schur complement to reformulate the first inequality constraint in (36) as

$$\mathbf{M}_{\text{opt}} = \begin{bmatrix} \gamma - \Theta_3 \mathbf{r} - \mathbf{r}^T \Theta_3^T - \Theta_2 & \mathbf{r}^T \\ \mathbf{r} & \Theta_1^{-1} \end{bmatrix} \succeq 0 \quad (37)$$

where \mathbf{M}_{opt} is denoted as the optimization matrix that minimizes the cost function for the minimal value of γ . It should be noted that \mathbf{M}_{opt} is linear in \mathbf{r} and γ .

The second inequality constraint that incorporates the constraints on the closed-loop signals can be rewritten as

$$\mathbf{M}_{\text{constr}} = \text{diag}(\mathbf{W}(\mathbf{k}^*) - \mathbf{Q} - \mathbf{L}\mathbf{r}) \succeq 0 \quad (38)$$

where $\text{diag}(\cdot)$ denotes a diagonal matrix that has the elements of the argument vector in its main diagonal. Finally, the resulting SDP yields

$$\begin{aligned} \min_{\mathbf{r}, \gamma} \quad & \gamma \\ \text{subject to} \quad & \begin{bmatrix} \mathbf{M}_{\text{opt}} & 0 \\ 0 & \mathbf{M}_{\text{constr}} \end{bmatrix} \succeq 0. \end{aligned} \quad (39)$$

G. Solution to LP, QP, and SDP Problems

A number of numerical techniques are available that solve LPs, QPs, and SDPs. Very efficient ways to solving those problems are based on primal-dual interior-point methods as shown in [26]. There it is noted that it is more efficient to solve the second-order cone programming problem which is a generalization of LP or QP rather than solving the more general SDP.

We will now show the effectiveness of the optimization routine proposed in Sections III-A–III-E by means of an illustrative application example: the seeking process in a hard disk drive. Both simulation and experimental results are presented that illustrate the effectiveness of closed-loop reference input shaping.

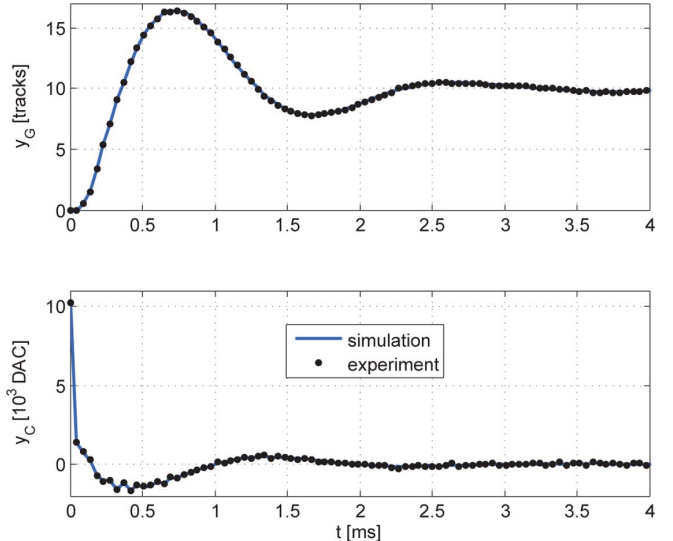


Fig. 6. Measured and simulated actuator (top) and controller (bottom) outputs for a closed-loop step of 10 tracks on r_1 .

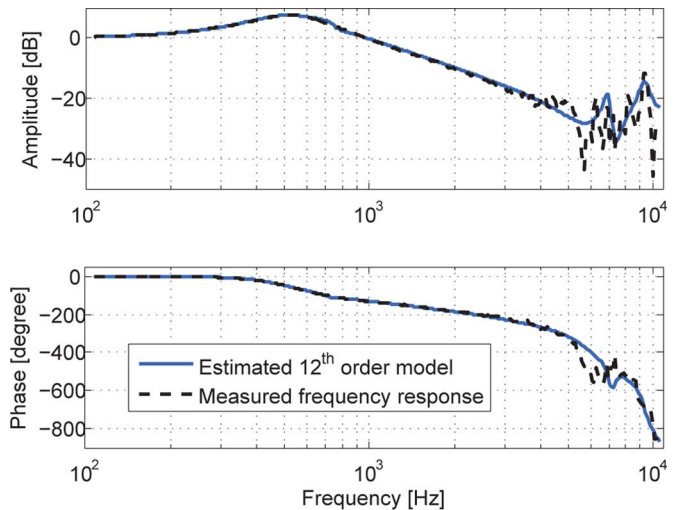


Fig. 7. Bode plot of estimated 12th-order model of the closed-loop transfer function and the measured frequency response from the HDD setup.

To solve such optimization problems, commonly used tools are the open source LMI parser YALMIP [27] and solver SeDuMi [28]. Our computations presented in the next subsection use the LP problem given in (31) to find feasible solutions for a specific \mathbf{k}^* . An optimal solution for the seek profiles for a given \mathbf{k}^* is then computed using the QP problem given in (32). For both LP and QP we use general SDP software based on MATLAB and the CVX software package [29].

IV. EXPERIMENTAL VERIFICATION: SEEKING IN A HDD

A. Experimental Set-Up

We consider an experimental set-up depicted in Figs. 4 and 5. A modified 3.5 inch form factor HDD spinning at 7200 rpm was used to experimentally verify the proposed optimization algorithm. As indicated in Fig. 4, a digital signal processing (DSP) board is connected to the HDD and a computer. The DSP board

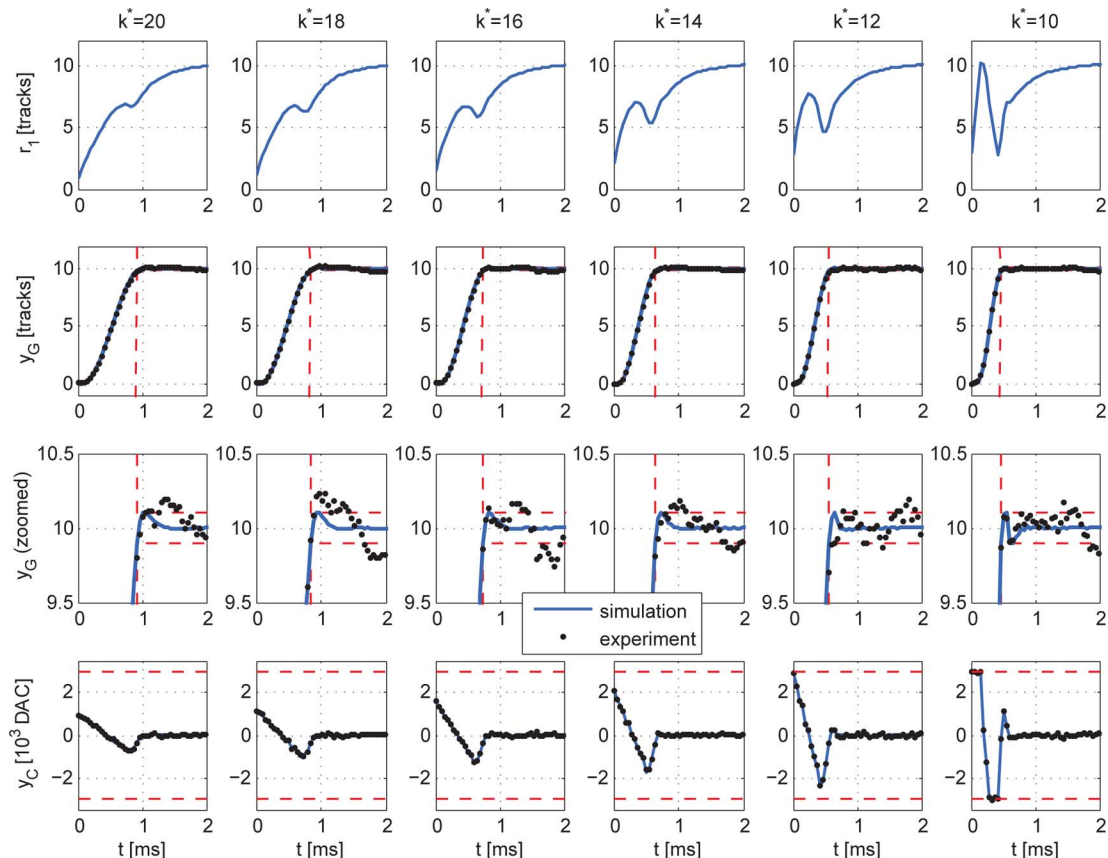


Fig. 8. Optimized reference signal r_1 (top row), output y_G (middle rows), and control signal y_C (bottom row) for 6 different sample numbers for k^* in simulation and actual experiment for a 10 track step. $k^* = 10$ samples represents the minimal time solution given the imposed constraints on y_C depicted by the dashed lines in the bottom row.

allows to gain access to HDD internal signals such as Gray code and position error signal (PES) in the drive. It also allows to inject pre-defined reference signals for seeking. The steps to obtain the experimental data are listed and indicated in Fig. 4. The HDD used for this study has 180 servo sectors which yields a PES/Gray code sampling frequency of 21.6 kHz. We consider a servo loop according to Fig. 1 where the dynamics of the HDD servo actuator—the voice coil motor (VCM)—are represented by G . Furthermore, a low bandwidth PID controller C is implemented for track-following. In order to compute optimized reference signals, the dynamic response of the servo loop needs to be identified. This was accomplished through step experiments described in Section IV-B.

B. Closed-Loop Dynamic Modeling of the Servo Mechanism

The state-space matrices A , B , C , and D in (8) can be formulated using explicit information of actuator and controller dynamics. Alternatively, since we are dealing with a closed-loop system, the matrices can also be formulated by directly studying the dynamics from reference signals to actuator output y_G and controller output y_C . For that purpose, a 10-track step on the reference signal r_1 was used to identify the dynamic behavior of the closed-loop system. For simplification, we neither consider r_2 nor constraints on δu_G in this study. It should be noted that the additional degree of freedom in r_2 is particularly useful

in control systems where the controller C incorporates a time-delay, and/or r_1 and r_2 are subjected individually to amplitude or rate constraints. For the conventional PID controller without delay and no constraints on r_1 and r_2 used in this study it is sufficient to only use r_1 . Considering those simplifications, the estimation problem reduces to a single-input ($r_1 \neq 0, r_2 = 0$) dual-output (y_G and $y_C = u_G$) system. A generalized realization algorithm (GRA) [30] was used to identify a discrete-time model based on the time-domain step response data. The step response measurement for both outputs is shown in Fig. 6. Based on the step data and the GRA a 12th-order closed-loop model was estimated. The simulated step response based on this model is also shown in Fig. 6 (solid lines). It can be observed that the estimated model captures the response of the system very well. Furthermore, a frequency domain comparison of the estimated model and a frequency response function measurement of the closed-loop transfer function (r_1 to y_G) based on sine sweep measurements was performed. The results are shown in Fig. 7. It can be seen that for low frequencies there is a strong agreement between measured and modeled response. However, high frequency resonance modes are not captured very well by the model. This is mainly due to the fact that the step input based modeling emphasizes on low frequency and most dominant resonance modes. We will see in Section IV-C that this does not have a large effect on the performance of the shaping algorithm as those high frequencies will not be excited by the

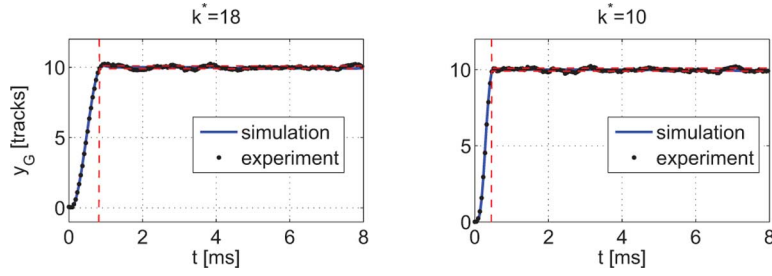


Fig. 9. Output y_G for sample number $k^* = 18$ and $k^* = 10$ in simulation and actual experiment for a 10 track step.

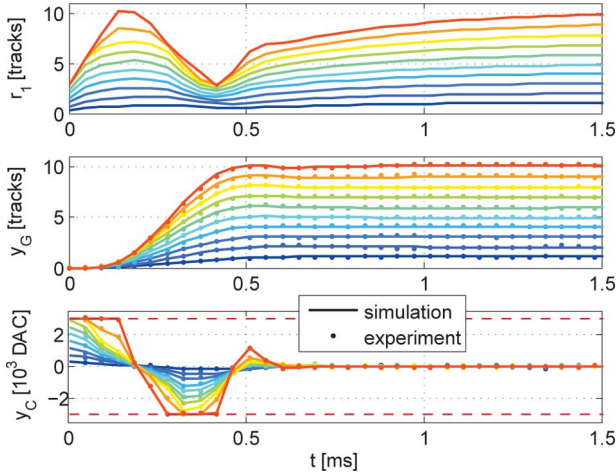


Fig. 10. Optimized reference signal r_1 (top), output y_G (middle), and control signal y_C (bottom) for different step sizes (1 to 10 tracks) at a fixed sample number of $k^* = 10$ in simulation and actual experiment.

shaped reference signal profile in closed-loop. In Fig. 7, the mismatch at higher frequencies between the frequency response measurement and the step input based model might also be caused by the different input signals. The frequency response measurement is based on a sine sweep input. In addition, the measurement could potentially be aliased.

C. Results

For our experimental studies we consider the reference signal r_1 and amplitude constraints on the control signal y_C which was set to a maximum absolute value of 3000 DAC units. The value ϵ was set to 10% of the track pitch which is a generally accepted limit in HDD technology. The difference between the output y_G and the target y_t was minimized along with the control signal $y_C = u_G$. No explicit constraints on the reference signal were considered by setting \mathbf{P}_2 in (32) to zero. For simplicity, the freedom in the scaling matrix \mathbf{P}_1 is not considered in our experimental results and \mathbf{P}_1 was defined as

$$\mathbf{P}_1 = \text{diag}(I_p, I_p, \dots, I_p), I_p = \begin{bmatrix} 1 & 0 & 0 \\ 0 & 1 & 0 \\ 0 & 0 & 0 \end{bmatrix} \quad (40)$$

to weigh y_G and u_G equally and not consider a rate of change δu_G . The experimental results are based on five averages of

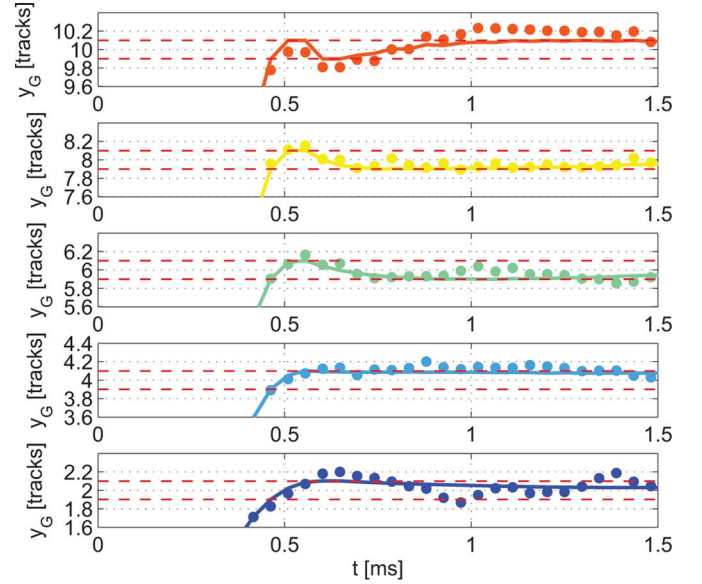


Fig. 11. Zoomed output y_G of Fig. 10 for even step sizes (2, 4, 6, 8, and 10 tracks) at a fixed sample number of $k^* = 10$ in simulation (solid lines) and actual experiment (dots).

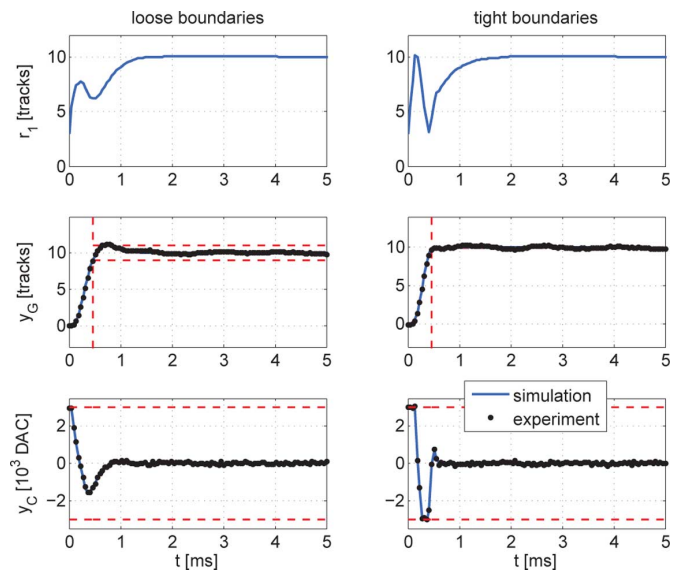


Fig. 12. Loose and tight output boundaries for a 10 track seek and $k^* = 10$ samples in simulation and experiment.

the measured signal. We will investigate the following four different cases:

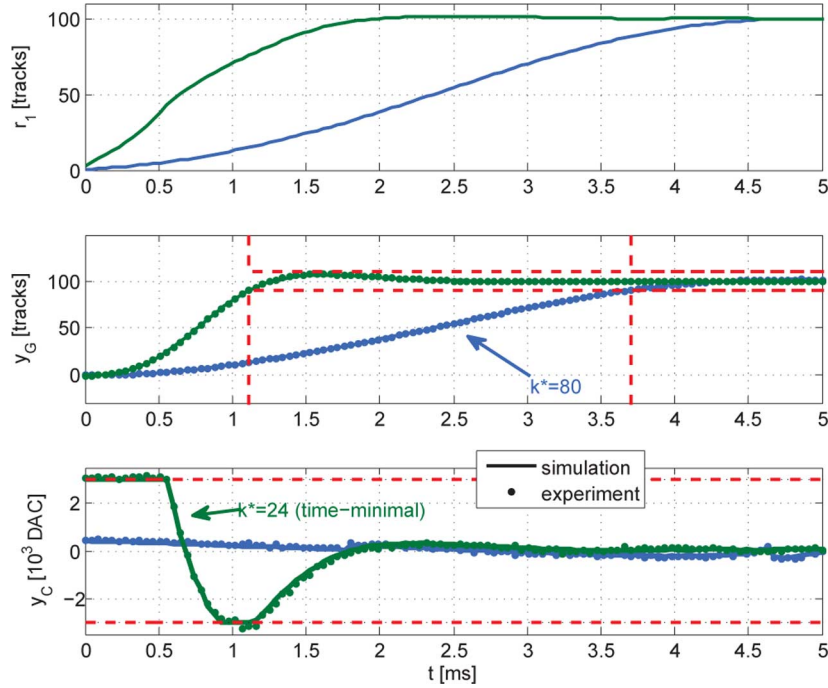


Fig. 13. 100 track step for loose boundaries and $k^* = 24$ (time-optimal) and $k^* = 80$ samples in simulation and experiment.

- 1) a fixed step size of 10 tracks and various settling times;
- 2) a variable step size combined with a fixed settling time of 10 samples;
- 3) tight versus loose amplitude constraints on y_G for 10 track step;
- 4) time-minimum solution versus a fixed settling time for a 100 track seek.

1) *Fixed Step Size and Various Settling Times:* In Fig. 8, the results for a fixed target track number of 10 tracks are shown. Each column in Fig. 8 represents a desired seek time ranging from 20 to 10 samples. It can be observed that the output y_G reaches the target much faster compared to the standard step input results in Fig. 6 and has no residual vibrations. It can also be observed that as the desired seek time approaches the time-minimum solution of 10 samples, the shape of the control output y_C looks very similar to “bang-bang” control which has been shown to be the time-optimal solution for an ideal double integrator actuator [31]. The additional resonance modes in the actuator require the control signal y_C to be slightly different from bang-bang and we accomplish this automatically by actual input shaping of the reference signal as plotted in the top row of Fig. 8. The zoom-in of the output y_G is shown in the third row of Fig. 8. One can observe that the experimentally obtained data follow the shaped output signal y_G of the actuator very closely. The violation of the imposed boundaries in the experimental data is due to repeatable and non-repeatable run-out errors (disturbances) that are poorly suppressed by the low bandwidth PID controller used in our experiments. In Fig. 9, we replot the output y_G over a longer time span than depicted in Fig. 8 for $k^* = 18$ and $k^* = 10$ which clearly shows stability of the closed-loop system. In addition, one can observe the repeatable components of the track run-out. An improved track-following controller could mitigate this effect but this is beyond the scope of this paper.

2) *Variable Step Size Combined With a Fixed Settling Time:*

In a second experiment, the settling time was set to the time-optimal solution of the 10 track step at 10 samples and the step size was varied from 1 to 10 tracks. The results are shown in Fig. 10. It is interesting to observe that the output y_G for each step height is just a scaled version of a different step height whereas y_C and r_1 are shaped accordingly. A zoomed version of the output y_G for even step sizes is shown in Fig. 11. Similar to the previous experiment, one can also observe small differences between measurement and simulation.

3) *Tight Versus Loose Amplitude Constraints on y_G :* We also investigated the difference between tight amplitude constraints on y_G (ϵ equals 10% of the track pitch) and loose constraints on y_G (ϵ equals 10% of the step height). The results in Fig. 12 show the time-optimal solution for both cases. Clearly, one can observe much smoother and less “aggressive” reference and control signals for the case of the loose constraint compared to the tight constraint.

4) *Time-Minimum Solution Versus a Fixed Settling Time:*

The final example shown in Fig. 13 considers a 100 track seek where the time-optimal solution is desired. Given the constraints on y_C , the target is reached within 24 samples. However, this yields large control signals that are saturated at the upper and lower boundaries for a significant amount of time. In addition, a slow seek to the same target was considered and a fixed settling time of 80 samples was assumed. One can observe in Fig. 13 that in this case the control signal is much smaller than for the time minimal seek which is expected. This might be of particular interest in a HDD as not always the time-minimum solution is desired. Moving the read/write head from one data sector (on track A) to the next data sector (on track B) might yield a fixed idle time due to the limited rotational speed of the disk. Since the idle time is known, one can compute an optimized control signal that minimizes the control energy and residual vibrations.

TABLE II
MATRIX DIMENSIONS

Symbol	row dimensions	column dimensions
A	$n_C + n_G + p$	
B	$n_C + n_G + p$	$m + p$
C	$m + 2p$	$n_C + n_G + p$
D	$m + 2p$	$m + p$
L	$4M(m + p) + 2N(m + 2p)$	$M(m + p)$
M	m	
M_{opt}	$M(m + p) + 1$	
M_{constr}	$4M(m + p) + 2N(m + 2p)$	
P₁	$N(m + 2p)$	
P₂	$M(m + p)$	
Ψ	$N(m + 2p)$	$M(m + p)$
Q, W	$4M(m + p) + 2N(m + 2p)$	1
q	$N(m + 2p)$	1
Θ₁	$M(m + p)$	
Θ₂	1	
Θ₃	1	$M(m + p)$
r	$M(m + p)$	1

V. CONCLUSION

An input shaping algorithm for closed-loop discrete-time LTI systems has been described in this paper. The algorithm was experimentally verified in a modified HDD setup showing excellent agreement between theoretical (simulation) and actual experimental results. It was shown that input shaping significantly reduces targeting time and residual vibrations compared to an output response obtained using standard reference signals such as steps. It was also shown that input shaping improves the response of systems whether or not plant saturation is present. Both the modeling and the reference signal shaping procedure are computational inexpensive and could be implemented in the firmware of a hard disk drive. This would allow adapting to variations due to tolerances in manufacturing and/or to changes in operating conditions. In addition, the reference signal shaping might significantly reduce seek-time, energy consumption, and system vibrations during the seeking process in an HDD.

APPENDIX SELECTED MATRIX DIMENSIONS

See Table II.

ACKNOWLEDGMENT

The authors would like to thank Headway Technologies Inc. for providing the experimental setup. Furthermore, they would like to express their gratitude to the anonymous reviewers for their comments that helped improving this manuscript.

REFERENCES

- [1] N. C. Singer and W. P. Seering, "Preshaping command inputs to reduce system vibration," *J. Dyn. Syst., Meas., Control*, vol. 112, no. 1, pp. 76–82, 1990.
- [2] J. Mattingly and S. Boyd, "Real-time convex optimization in signal processing," *IEEE Signal Process. Mag.*, vol. 27, no. 3, pp. 50–61, May 2010.
- [3] L. Y. Pao, "Multi-input shaping design for vibration reduction," *Automatica*, vol. 35, no. 1, pp. 81–89, 1999.
- [4] M. D. Baumgart and L. Y. Pao, "Discrete time-optimal command shaping," *Automatica*, vol. 43, no. 8, pp. 1403–1409, 2007.

- [5] V. Kapila, A. Tzes, and Q. Yan, "Closed-loop input shaping for flexible structures using time-delay control," *J. Dyn. Syst., Meas., Control*, vol. 122, no. 3, pp. 454–460, 2000.
- [6] L. Y. Pao and C. La-orpacharapan, "Shaped time-optimal feedback controllers for flexible structures," *J. Dyn. Syst., Meas., Control*, vol. 126, no. 1, pp. 173–186, 2004.
- [7] K. Kogiso and K. Hirata, "Reference governor for constrained systems with time-varying references," *Robot. Autonomous Syst.*, vol. 57, no. 3, pp. 289–295, 2009.
- [8] C. Cutforth and L. Pao, "Control using equal length shaped commands to reduce vibration," *IEEE Trans. Control Syst. Technol.*, vol. 11, no. 1, pp. 62–72, Jan. 2003.
- [9] Z. Masoud and M. Daqaq, "A graphical approach to input-shaping control design for container cranes with hoist," *IEEE Trans. Control Syst. Technol.*, vol. 14, no. 6, pp. 1070–1077, Nov. 2006.
- [10] K. Sorensen, K. Hekman, and W. Singhose, "Finite-state input shaping," *IEEE Trans. Control Syst. Technol.*, vol. 18, no. 3, pp. 664–672, May 2010.
- [11] T. Sugie and H. Yamamoto, "Reference management for closed loop systems with state and control constraints," in *Proc. Amer. Control Conf.*, 2001, pp. 1426–1431.
- [12] H. Suzuki and T. Sugie, "Off-line reference shaping of periodic trajectories for constrained systems with uncertainties," *IEEE Trans. Autom. Control*, vol. 53, no. 6, pp. 1531–1535, 2008.
- [13] T. Sugie and H. Suzuki, "Reference shaping of periodic trajectory for systems having constraints," in *Proc. Amer. Control Conf.*, 2004, pp. 4657–4662.
- [14] L. Van de Broeck, M. Diehl, and J. Swevers, "Embedded optimization for input shaping," *IEEE Trans. Control Syst. Technol.*, vol. 18, no. 5, pp. 1146–1154, Sep. 2010.
- [15] B. Chen, T. Lee, and V. Venkatakrishnan, *Hard Disk Drive Servo Systems*, ser. Advances in Industrial Control. New York: Springer, 2002.
- [16] M. L. Workman, R. L. Kosut, and G. F. Franklin, "Adaptive proximate time-optimal servomechanisms: Continuous time case," in *Proc. Amer. Control Conf.*, 1987, pp. 589–594.
- [17] T. Yamaguchi, K. Shishida, S. Tohyama, and H. Hirai, "Mode switching control design with initial value compensation and its application to head positioning control on magnetic disk drives," *IEEE Trans. Ind. Electron.*, vol. 43, no. 1, pp. 65–73, Feb. 1996.
- [18] T. Yamaguchi, H. Numasato, and H. Hirai, "A mode-switching control for motion control and its application to disk drives: Design of optimal mode-switching conditions," *IEEE/ASME Trans. Mechatron.*, vol. 3, no. 3, pp. 202–209, Sep. 1998.
- [19] B. Chen, T. Lee, K. Peng, and V. Venkataramanan, "Composite nonlinear feedback control for linear systems with input saturation: Theory and an application," *IEEE Trans. Autom. Control*, vol. 48, no. 3, pp. 427–439, Mar. 2003.
- [20] M. Hirata and M. Tomizuka, "Short track seeking of hard disk drives under multirate control-computationally efficient approach based on initial value compensation," *IEEE/ASME Trans. Mechatron.*, vol. 10, no. 5, pp. 535–545, Oct. 2005.
- [21] G. Goodwin, M. Seron, and J. de Dona, *Constrained Control and Estimation: An Optimization Approach*. London, U.K.: Springer Verlag, 2005.
- [22] S. Boyd and L. Vandenberghe, *Convex Optimization*. New York: Cambridge Univ. Press, 2004.
- [23] J. Nocedal and S. J. Wright, *Numerical Optimization*. New York: Springer-Verlag, 1999.
- [24] O. N. Starnes and R. A. de Callafon, "Time-optimal input shaping for discrete-time lti systems with application to seek profiles of a hdd system," in *Proc. ASME ISPS Conf.*, 2007, pp. 146–148.
- [25] L. Vandenberghe and S. Boyd, "Semidefinite programming," *Soc. for Ind. Appl. Math. Rev.*, vol. 38, no. 1, pp. 49–95, 1996.
- [26] M. S. Lobo, L. Vandenberghe, S. Boyd, and H. Lebret, "Applications of second-order cone programming," *Linear Algebra its Appl.*, pp. 193–228, 1998.
- [27] J. Lofberg, "Yalmip: A toolbox for modeling and optimization in MATLAB," in *Proc. CACSD Conf.*, 2004, pp. 284–289.
- [28] J. F. Sturm, "Using Sedumi 1.02, A Matlab Toolbox for Optimization Over Symmetric Cones," 1999.
- [29] M. Grant and S. Boyd, "CVX: Matlab Software for Disciplined Convex Programming, Version 1.21," 2010.
- [30] R. A. de Callafon, B. Moaveni, J. P. Conte, X. He, and E. Udd, "General realization algorithm for modal identification of linear dynamic systems," *J. Eng. Mechan.*, vol. 134, no. 9, pp. 712–722, 2008.
- [31] A. A. Mamun, *Hard Disk Drive: Mechatronics and Control; Electronic Version*. Hoboken, NJ: CRC Press, 2006.



Uwe Boettcher (S'08) received the Dipl.-Ing. degree (corresponding to M.Sc.) in electrical engineering from Dresden University of Technology, Dresden, Germany, in 2008 and the M.Sc. and Ph.D. degrees in mechanical engineering from University of California at San Diego, La Jolla, in 2010 and 2011, respectively.

He is currently with Daimler AG, Sindelfingen, Germany. He studied electrical engineering from 2003 to 2008. In 2005, he specialized in precision mechanics. He joined Prof. Talke's Group in 2007.



Dirk Fetzer received the B.Sc. degree in physics from the University of Goettingen, Goettingen, Germany, in 2009. He is currently pursuing the M.Sc. degree in electrical engineering from RWTH Aachen, Aachen, Germany.

From 2009 to 2010, he was part of the Education Abroad Program of the University of California at San Diego, La Jolla. During the Spring and Summer of 2010 he worked as a visiting graduate student in the research group of Professor Talke at the Center for Magnetic Recording Research. He was an intern

with Robert Bosch GmbH.



Hui Li received the Bachelor's degree in mechanical science and engineering and economics and the Master's degree in mechanical science and engineering from the Huazhong University of Science and Technology (HUST), Huazhong, China, in 1999 and 2002, respectively, and the Ph.D. degree in electrical and computer engineering from National University of Singapore (NUS), Data Storage Institute (DSI), Singapore, in 2007.

From August 2005 to January 2008, he was with the Mechanical Storage Laboratory, R&D Center, Hitachi Asia Ltd., Singapore. From June 2006 to December 2006, he was appointed to work with the HD Unit, Central Research Laboratory, Hitachi Ltd., Japan. In 2008, he was with Prof. Talke's Group in the area of numerical modeling of the head-disk interface. Since 2009, he has been with the Mechanical Storage Laboratory, R&D Center, Hitachi Asia Ltd., Singapore.



Raymond A. de Callafon received the M.Sc. and Ph.D. degrees in mechanical engineering from the Delft University of Technology, Delft, The Netherlands, in 1992 and 1998, respectively.

From 1997 to 1998, he was a Research Assistant with the Structural Systems and Control Laboratory, Mechanical and Aerospace Engineering Department, University of California at San Diego, La Jolla. Since 1998, he has been a Professor with the Dynamic Systems and Control Group, University of California at San Diego. His research interests include topics in the field of control relevant system identification, structural damage detection, (linear) feedback control design, model/controller reduction and identification, and real-time control problems applied to high-precision data storage systems and active noise and vibration control applications.



Frank E. Talke (F'06) received the Dipl.-Ing. degree from the University of Stuttgart, Stuttgart, Germany, in 1965 and the M.Sc. and Ph.D. degrees from the University of California, Berkeley, in 1966 and 1968, respectively.

From 1969 to 1986, he was with the IBM Research and Development Laboratories, San Jose, CA, and in 1984 he spent one year as a guest Professor with the University of California, Berkeley. He accepted a position as an Endowed Chair Professor at the Center for Magnetic Recording Research (CMRR) effective March, 1986. He is the author of more than 290 publications and holds 11 U.S. patents. His research interests include the areas of the head/disk and head/tape interface, tribology, mechanical design related to magnetic recording technology, and high precision instrumentation.

Prof. Talke is a Fellow of the ASME and the STLE. He was a recipient of the ASME Medal in 2008, the Humboldt Research Price in 2007, the Mayo D. Hersey Award in 2010, and the Tribology Gold Medal in 2011. He was elected a member of the National Academy of Engineering in 1999.